Aalborg Universitet

Aalborg University
DENMARK

Optimisation of Electrochemical Deposition of Calcareous Material During Cathodic Protection by Implementing Response Surface Methodology (RSM)

Sharker, Tanzila; Simonsen, Kenneth René; Margheritini, Lucia; Kucheryavskiy, Sergey; Simonsen, Morten Enggrob

Link to publication from Aalborg University

Contents lists available at ScienceDirect

Electrochimica Acta

Optimisation of electrochemical deposition of calcareous material during cathodic protection by implementing response surface methodology (RSM)

Tanzila Sharker [a], Kenneth R. Simonsen [a], Lucia Margheritini [b], Sergey V. Kucheryavskiy [a], Morten E. Simonsen [a],*

[a] Department of Chemistry and Bioscience, Aalborg University, Niels Bohrs Vej 8, 6700, Esbjerg, Denmark
[b] Department of Build Environment, Aalborg University, Thomas Manns Vej 23, 9220, Aalborg, Denmark

ABSTRACT

This paper investigates the deposition of calcareous material on carbon steel through cathodic protection. A Response Surface Methodology (RSM) was applied to model the electrodeposition of calcareous material in ASTM seawater by varying temperature and current density parameters. The calcareous deposit was more compact at a current density $\leq 150\ \mu A/cm^2$. At least $55\ \mu A/cm^2$ current density was required to provide cathodic protection and initiate electrodeposition, thus inhibiting corrosion. Furthermore, the produced RSM models can predict the amount and composition of the material at $55 - 310\ \mu A/cm^2$ current density and $4 - 25\ °C$ temperature.

1. Introduction

Electrochemical deposition of calcareous material in seawater can provide strength to offshore structures similar to steel reinforced concrete. The calcareous deposit mainly consists of calcium carbonate ($CaCO_3$) and magnesium hydroxide ($Mg(OH)_2$). Deposition of calcareous material during cathodic protection (CP) on large static steel structures such as wind turbines, wave energy substructures, and offshore oil and gas platforms enhances their lifespan [1,2]. The primary construction material for those substructures is carbon steel, which requires protection for providing safe long-term operation. The calcareous coating on offshore wind turbine monopile can potential protect against corrosion, biofouling, and erosion [1–8].

A potential between $-0.8\ V$ to $-1.1\ V$ versus Ag/AgCl electrode is an acceptable range for providing adequate protection against corrosion [9]. The efficiency of CP tends to be enhanced by the deposition of calcareous material on the polarised structure. The calcareous deposit acts as a barrier to oxygen diffusion towards the metal structures. Therefore, it limits the cathodic oxygen reduction reaction on the polarised surface, thus decreasing the required current [2,10]. It can be explained as the resistance tends to increase with the growing thickness of the calcareous deposit on the cathode surface thus, the current tends to decrease if the applied potential is constant [2,3,4].

During CP, dissolved oxygen near the polarised surface is reduced, thus generating hydroxyl ions (OH^-) and increasing the interfacial pH. As a result, the concentration of carbonate ions (CO_3^{2-}) increases, contributing to the precipitation of $CaCO_3$ based minerals. In addition, the magnesium ions present in the seawater also react with OH^- ions near the polarised surface, hence forming $Mg(OH)_2$ also known as brucite along with $CaCO_3$ [1–3,7,8,11–13]. About 2 cm thick layers of calcareous deposits can be grown per year, the material growing under cathodic polarisation gets stronger with age, is self-repairing, and it can be several times harder than Portland Cement concrete [2,14,15]. The presence of aragonite polymorph of $CaCO_3$ is the main contributor for enhancing the strength of the material formed under CP, whereas brucite is a much softer material compared to aragonite [4]. The deposit tends to get stronger over time with an increase in aragonite percentage. A field test conducted by Margheritini et al. [2] reported through XRD analysis that there was an increase of aragonite percentage in the mineral composition from 65.9 to 75.8% within a period of 2 weeks to 3 months. It was also found that the material was strengthened in both cold and warm water conditions. Research carried out by Johra et al. [16] showed that calcareous material can have mechanical resistance similar to concrete. A material composed of 80.8% aragonite, 18.9% brucite, and 0.3% calcite produced at 2.5 V had a compressive strength above 3.5 kN, similar to concrete with a grade class C20/25. It had a very compact structure with pore volumes of $\leq 1\ \mu m$ (microporous).

There are numerous studies conducted primarily focusing on

understanding the formation mechanism of calcareous material [2–5,7, 17–19]. The growth of calcareous deposit under CP is highly influenced by several factors such as the applied cathodic potential, current, temperature, pressure, pH, and seawater composition.

Barchiche et al. [4] studied the effects of temperature on the deposit, which indicated that the influence of temperature also depends on the applied potential. Low temperature can favour the aragonite formation at moderately low negative cathodic potential (−1.0 V/SCE), where this phenomenon is governed by the solubility of CaCO$_3$. Conversely, the formation of brucite is more favourable at −1.2 V/SCE cathodic potential, where interfacial pH is the controlling factor for deposition. A study by Margheritini et al. [2] also found that applied current has a major influence on the growth rate and composition of deposit material. The low current favoured aragonite formation, whereas increasing current resulted in a more porous structure mainly by increasing the formation of brucite. Another study by Cooke et al. [19] found that water chemistry can significantly influence the solubility of aragonite. It indicated that the carbonate ion concentration is the dominant controlling factor on the apparent solubility product of aragonite, which is a function of pH.

This paper focused on investigating the influence of temperature and current density on the electrochemical deposition of calcareous material in artificial seawater in a controlled environment. The experiments were planned using core principles of statistical design of experiments, which makes it possible to resolve the effects of different factors and evaluate possible interaction between them. The optimisation part is done using response surface methodology (RSM) and central composite design (CCD) where current and temperature were the main factors while the amount of calcareous material produced and aragonite percentage in the deposit were the response variables.

2. Materials and methods

2.1. Materials

Sodium chloride (NaCl, 100%), Calcium chloride (CaCl$_2$, 90–98%), Potassium chloride (KCl, 97%) and Magnesium chloride hexahydrate (MgCl$_2$·6H$_2$O, >97%) were purchased from VWR Chemicals BDH (Leuven, Belgium). Sodium sulfate (Na$_2$SO$_4$, ≥99%) and Sodium hydroxide (NaOH, ≥99%) were obtained from Sigma-Aldrich (Darmstadt, Germany). Sodium hydrogen carbonate (NaHCO$_3$, 99%) was acquired from Alfa Aesar (Kandel, Germany).

2.2. Electrolyte and electrochemical parameters

The experiments were conducted using synthetic seawater as the electrolyte solution. The seawater was prepared according to the standard solution of marine water provided by the American Society and Materials (ASTM D1141) [2,20]. The composition of the artificial seawater is shown in Table 1. The water was prepared in 100 L batches. At first, NaCl, CaCl$_2$, Na$_2$SO$_4$, KCl and NaHCO$_3$ salts were dissolved in 50 L of deionised water in a 100 L barrel. Then, MgCl$_2$·6H$_2$O was added to the mixture and the barrel was filled up with deionised water to 100 L. Finally, the pH of the seawater was adjusted to ~8.2 by the addition of 1 M NaOH.

Table 1
Chemical composition of artificial seawater based on ASTM D1141 [2,20].

| Component	Concentration [g/L]
NaCl	24.530
MgCl$_2$·6H$_2$O	11.128
Na$_2$SO$_4$	4.090
CaCl2	1.160
KCl	0.695
NaHCO$_3$	0.201

A schematic illustration of the experimental laboratory setup is shown in Fig. 1. The electrochemical cell used for the experiment consisted of a plastic tank (22cm×33cm×15 cm) containing ~11 L seawater. The tank was connected to a reservoir thus continuously pumping seawater with a flowrate of ~500 mL/h to maintain a constant electrolyte solution composition near the cathode surface. The water inlet and outlet were placed 4 and 15 cm from the bottom of the tank, respectively. Pumping the water at a constant rate provided a continuous supply of ions, thus helping maintain the tank's pH. A constant slow stirring was provided to maintain a homogeneous solution. A refrigerator was used to keep the temperature of the water below ambient (22 °C) for the experiments, whereas a heating rod was used to provide temperature above ambient.

A powerbox LBX 30–200 (0–30 V, 0–200A) was used for providing constant current. Carbon steel plates (DC01 AM) of 2 mm thickness were used as cathodes with an exposed area of 100.4 cm^2 in the seawater, whereas a dimensionally stable anode (DSA) with an exposed area of 77.2 cm^2 was used as a counter electrode. Four identical parallel setups were connected to the power supply and ran at the same time. The power supply provided a set current, split into four parallel setups. The actual current provided to each of the four parallel electrochemical systems was measured during the experiment.

The DSA anode consisted of a titanium plate covered with mixed metal oxide, which is an inert anode material optimised for oxygen reaction (Electrocell MFC40032-Ti-DSA-O2). A constant distance of 17 cm between the anode and the cathode was maintained for all experiments. A thin layer of silicon was used to cover the unexposed area of cathodes. Prior to the experiments, the cathodes were moderately washed in 1 M HCl acid and rinsed with deionised water, followed by drying. The weight of the cathodes after applying the silicon layer on the unexposed area was measured before starting the experiment. The duration of each experiment was 14 days. At the end of each experiment, the cathode was gently washed in deionised water to avoid the deposition of NaCl crystals from the seawater and dried at 60 °C. Finally, the weight of the dried cathode was measured and mass of produced material was calculated.

2.3. Response surface methodology and central composite design

Response surface methodology (RSM) is an efficient tool for finding optimal values of two or more factors to reach the maximum or minimum response characteristic of a process or a reaction. In this work, RSM was applied to maximise the calcareous deposit and the percentage of aragonite by varying the temperature and current. Through RSM, a response is described by a surface defined by the Taylor equation (cf. Eq. (1)). The equation is used for approximating any continuous function by a power series in a limited design space (range of X1 and X2).
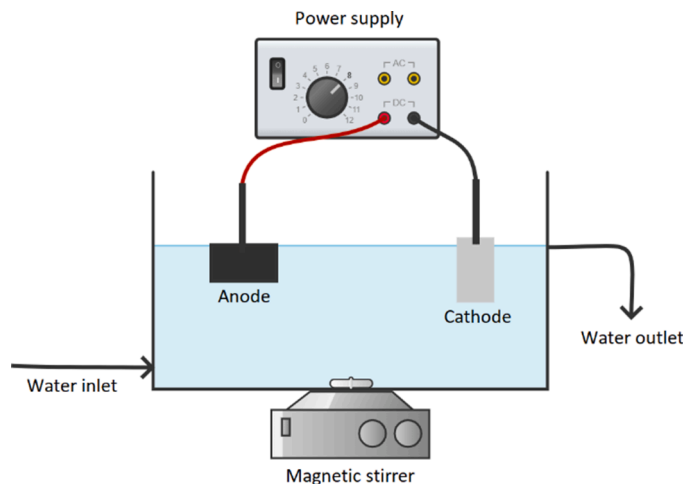
Fig. 1. Overview of the experimental setup.

$$Response = b_0 + b_1X_1 + b_2X_2 + b_3X_1X_2 + b_4X_1^2 + b_5X_2^2 \qquad (1)$$

Here b_0, b_1, …, b_5 are coefficients determined by experimental data obtained using the Box-Wilson Central Composite Design (CCD) [21,22]. X_1 and X_2 are linear terms for current and temperature, respectively. X_1^2 and X_2^2 are the nonlinear squared terms for current and temperature, respectively. The $X_1 \times_2$ is the interaction term. The experiments were carried out using circumscribed, CCD (cf. Fig. 2) which contains an embedded 2^k (where $k = 2$, number of variables) four factorial design points with its origin at the centre augmented with four outer points fixed axially at a distance α from the centre. Five replications of experiments for the centre point were performed to provide a reliable estimation of the experimental error. The CCD design is fully rotatable, meaning that the uncertainty at a given distance from the centre point is the same regardless of direction.

The total number of experiments required for the RSM with two factors is 13 (cf. Table 2). The value of α was chosen to maintain rotatability by ensuring a constant variance of the predicted model at all points equidistant from the design centre [22,23]. The coded levels of the factors are ± 1 for the factorial points, 0 for the centre points and $\pm\alpha$ (± 1.414) for the outer points. The value of α was calculated based on the number of experimental runs in the factorial portion of the CCD as shown in Eq. (2).

$$\alpha = \left[2^k\right]^{\frac{1}{4}} \qquad (2)$$

The experiments were carried out in random order, for each experiment the amount of calcareous deposit and the percentage of aragonite was measured and stored in the data table. After that, a regression analysis was carried out on each response to estimate the model (cf. Eq. (1)), standard error and significance [23]. All calculations and visualisations were performed using MATLAB v. R2019a (The MathWorks Inc., Natick, Massachusetts).

2.4. X-Ray diffraction (XRD) and X-Ray fluorescence (XRF)

After collecting the deposited material from the cathode, the composition was analysed through XRD using a PANalytical AERIS diffractometer. The diffractometer used a Cu K-alpha radiation source (wavelength $\lambda = 1.54$ Å) with a Ni filter and operated at 40 kV and 15 mA. The samples were scanned from 15 to 90° 2θ angle with the time constant set to 12 min. Rietveld refinement using PANalytical HighScore Plus was used to determine the fractions of minerals in the samples.
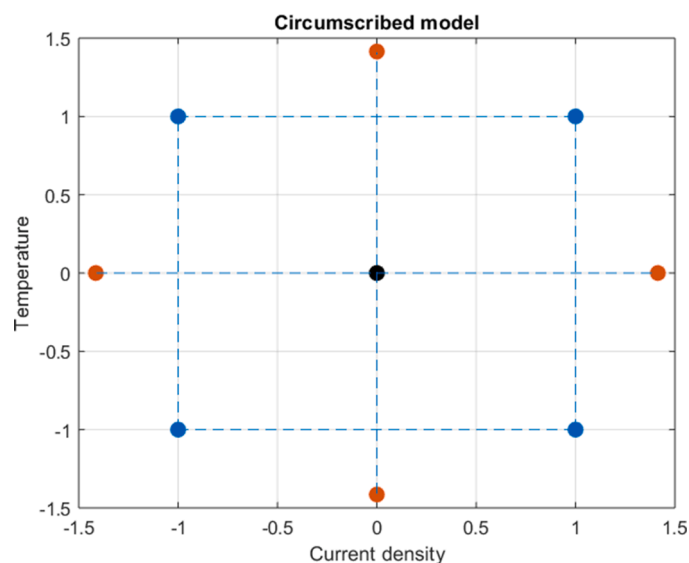

Fig. 2. - The Circumscribed model, consisting of central points (black), corner points (blue) and outer points (orange).

Table 2

Overview of the factors and levels (Coded and Actual levels) used in the experiment are presented. F1-F4, C1-C5, and O1-O4 are the full factorial design points, the central point and the outer points, respectively.

Experiment	Coded levels		Actual levels	
	Temperature	Current density	Temperature [°C]	Current density [μA/cm²]
F1	1	1	22	265
F2	1	−1	22	55
F3	−1	1	7	265
F4	−1	−1	7	55
C1				
C2				
C3	0	0	14	150
C4				
C5				
O1	−1.414	0	4	150
O2	1.414	0	25	150
O3	0	1.414	14	310
O4	0	−1.414	14	0

Furthermore, a Rigaku-Supermini200 XRF instrument was used for elemental analysis of the deposit materials. The XRF used a helium atmosphere with a 50 kV Pd X-Ray tube.

2.5. Scanning electron microscopy (SEM) and energy dispersive X-Ray analysis (EDX)

The surface of the cathodes with deposited material was observed through a Zeiss Evo 60 SEM instrument operating at 10 kV. The aragonite and brucite crystals formed on the cathodes were identified through SEM micrographs. Furthermore, the X-Ray technique attached to the SEM instrument known as EDX was used for the elemental mapping of the samples.

2.6. Adhesive test

The adhesion between the calcareous material and the steel cathode was analysed using a 180° peel test applying a Lloyd LR50 plus with a 500 N load cell. The peel test was caried out using a VHB Acrylic foam tape from 3 M (5952) with a width of 25.4 mm. The test speed was 40 mm/min.

3. Results and discussion

The elemental quantification and composition of the deposit materials obtained through XRF and XRD analyses, respectively, are presented in Table 3. The iron content in the deposits acquired through XRF can be used for identifying the occurrence of corrosion during the experiments.

The experimental results (cf. Table 3) show that the highest amount of calcareous deposit (9.9 g) was produced at 265 μA/cm² and 22 °C with an aragonite percentage of 1.5%, which is the lowest measured value of aragonite in the dataset. The second lowest measurement of aragonite (2.6%) was observed at the same current, 265 μA/cm² and at 7 °C with a 2.5 times lower deposit weight (4.0 g). This indicates that temperature greatly influences the amount of calcareous deposit formed on the cathode.

Additionally, comparing the two current densities 265 and 55 μA/cm² at 22 °C, F1 and F2, respectively. The percentage of aragonite increased from 12.1% to 67.0% with the decrease in current density, however with a reduction in weight from 9.0 g to 1.6 g (cf. Table 3). The same trend was observed for F3 (265 μA/cm²) and F4 (55 μA/cm²) at 7 °C, where a decrease in current from 265 μA/cm² led to a growth of the aragonite percentage from 16.1% to 85.6% but at the same time the amount of calcareous deposit had fallen from 6.5 g to 1.1 g. From this it can be concluded that a larger current reduces the percentage of

Table 3
The weight of deposit on the cathode and the percentage of aragonite.

Experiment	Temperature [°C]	Current density [μA/cm^2]	Weight [g]	Weight [g/cm^2]	Aragonite [%]	Brucite [%]	XRF [%]
F1	22	265	9.03	0.090	12.1	87.9	Ca: 20.3 Mg: 70.6 Fe: 2.5
F2	22	55	1.57	0.016	67.0	33.0	Ca: 59.3 Mg: 34.0 Fe: 3.93
F3	7	265	6.53	0.065	16.1	84.0	Ca: 27.6 Mg: 65.8 Fe: 1.6
F4	7	55	1.14	0.011	85.6	14.4	Ca: 76.1 Mg: 14.8 Fe: 7.03
C1	14	150	5.48	0.055	15.8	84.2	Ca: 38.6 Mg: 57.2 Fe: 0.351
C2	14	150	5.57	0.055	18.5	81.5	Ca: 32.6 Mg: 62 Fe: 0.513
C3	14	150	6.13	0.061	20.0	80.0	Ca: 25.1 Mg: 68.0 Fe: 0.582
C4	14	150	4.66	0.046	22.6	77.5	Ca: 36.2 Mg: 57.7 Fe: 0.283
C5	14	150	4.62	0.046	20.3	79.7	Ca: 21.7 Mg: 73.9 Fe: 0.615
O1	4	150	2.35	0.023	33.6	66.4	Ca: 46.2 Mg: 49.3 Fe: 0.896
O2	25	150	6.97	0.069	13.5	86.5	Ca: 25.1 Mg: 69.7 Fe: 0.891
O3	14	310	8.84	0.088	11.2	88.8	Ca: 20.6 Mg: 72.0 Fe: 0.511
O4	14	0	*	*	*	*	*

* Too low current to initialise the electrolysis.

aragonite in the deposit, however enhancing the production of the material. Additionally, a high temperature lowers the formation of aragonite but increases the total weight of the material. Comparing F1
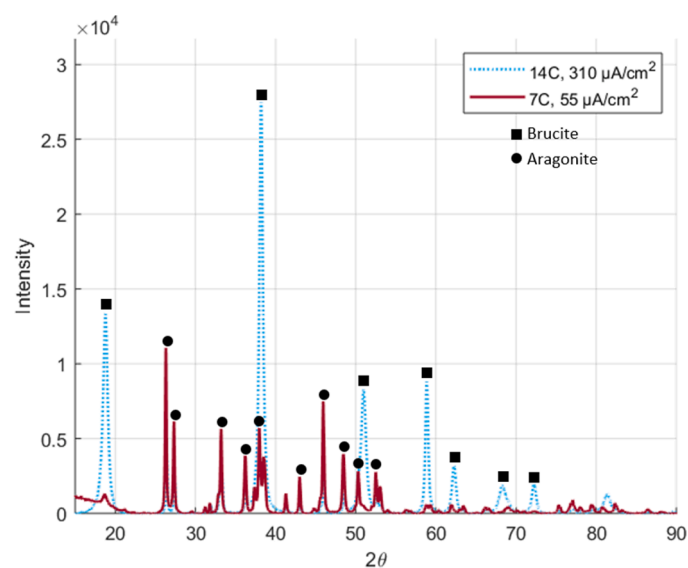
Fig. 3. The XRD spectra of the calcareous material produced at 310 μA/cm^2, 14 °C (F1, marked with blue), and 55 μA/cm^2, 7 °C (F4, marked with red). The composition of aragonite and brucite for the F1 is 11.2% and 88.8%, respectively and 85.6% and 14.4% for F4, respectively.

and F4, the XRD spectra can be observed in Fig. 3 showing a higher intensity of the brucite peaks for F1 conducted at a higher current density (310 μA/cm^2). Additionally, the intensity of the brucite peaks is low for F4 at 55 μA/cm^2 meanwhile the aragonite peaks have higher intensity.

The XRD analysis of the five centre point samples (C1-C5) produced at 150 μA/cm^2 and 14 °C showed that the average percentage of aragonite is 19.4 ± 2.49%. Additionally, the weight of the samples is 0.053±0.01 g/cm^2.

Comparing O1 and O2 which were conducted at 4 and 25 °C, respectively at a current density of 150 μA/cm^2. The percentage of aragonite in the deposit was reduced to more than half when elevating the temperature from 4 to 25 °C, however increased the amount of deposit by three times. Observing the samples in Fig. 5C and D, a thinner and less dense layer of the calcareous deposit was observed at a lower temperature compared to the higher temperature. Additionally, the structure of the deposit was porous due to hydrogen bubbles formed underneath the calcareous deposit.

Since the experiments were conducted under low stirring, it could have contributed to a higher amount of brucite and a flaky structure of some of the samples. Studies [6,24] found that during cathodic protection of a steel plate in a stirred environment favoured aragonite formation with a thinner layer compared to a stagnant environment. In addition, a higher stirring contributed to the evacuation of OH$^-$ ions from the cathode surface, thus not increasing the pH and hindering the Mg(OH)$_2$ precipitation.

The plot in Fig. 4 represents the data as aragonite percentage vs weight in g/cm^2 with the standard deviation calculated from the central
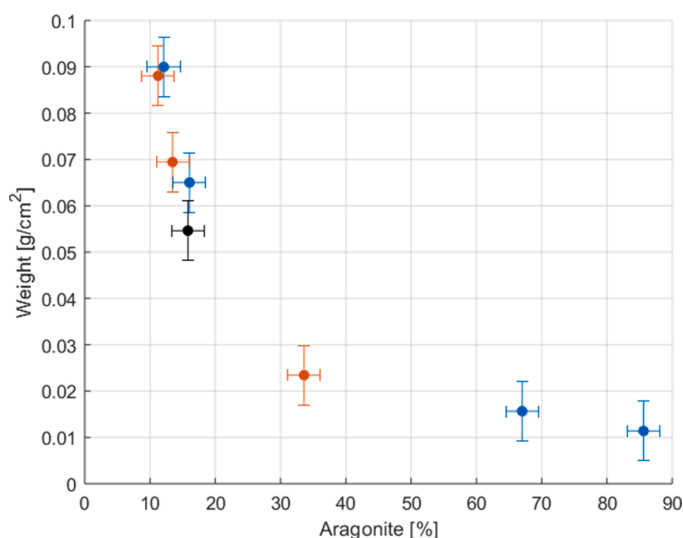
Fig. 4. The two responses aragonite (%) and weight of calcareous material shown as a scatterplot with the standard deviation calculated from the central point experiments. Corner points (blue), outer points (orange) and mean of centre points (black).

point experiments. The data shows a negative exponential trend where aragonite is inversely proportional to the weight.

Conducting the experiment at an applied current lower than 55 μA/cm^2 resulted in corrosion of the cathode instead of gaining a calcareous deposit on the surface. Therefore, no cathodic protection was observed for outer point O4 at ~0 μA/cm^2 and 14 °C. The reason for the corrosion building up on the cathode at <55 μA/cm^2 is a result of a potential less than the required overpotential to initiate the redox reaction with the electrolyte (ASTM). As an example, the voltage for the centre experiments (C1-C5) at 150 μA/cm^2 and 14 °C stabilised at a potential of 2.28 V after 24 h but increased to 2.31 V over 14 days. However, when conducting the experiments at <55 μA/cm^2, the voltage did not stabilise but decreased to ~0.06 V after 24 h.

Furthermore, the deposition of calcareous material was a slow process for the carbon steel plate cathodically protected at 55 μA/cm^2 at both temperatures 22 and 7 °C. A visual inspection of the cathodes with deposits showed an indication of corrosion at such low current. The presence of brown/orange spots underneath the white deposit layer was visually observed (cf. Fig. 5A). However, the corrosion only occurred at the initial stage of the experiment in the absence of calcareous material. The corrosion was eventually controlled when the material started forming on the cathode. The XRF analysis showed a 3.93 and 7.03% iron content in the deposit materials obtained at 22 and 7 °C (at 55 μA/cm^2), respectively. Additionally, a small amount of iron (<1%) was measured in some samples which could be from the cathode while collecting the calcareous deposit. A study by Yang et al. [3] reported a clear correlation between the iron containing corrosion products and overlying brucite layer at cathodic current densities ranging between 50 and 100 μA/cm^2. A thin inner magnesium layer incorporated with iron was observed at the beginning, which was eventually followed by a thick outer calcium carbonate layer. The study also reported that at current densities ranging from 150 to 200 μA/cm^2 the deposited material consisted of a magnesium rich inner layer and a calcium rich outer layer.

Furthermore, this study observed a higher tendency of cracking and flaky structure leading to a lower material cohesion in the deposits acquired at a high current density of 310 μA/cm^2. The occurrence of severe hydrogen (H$_2$) gas bubbling through nanopores of the deposits resulted in increased cracking. Intense bubbling resulted from a high level of alkalisation near the metal surface. The material produced at 310 μA/cm^2 consisted of 88.8% brucite and 11.2% aragonite with a total mass of 8.84 g material after 14 days.
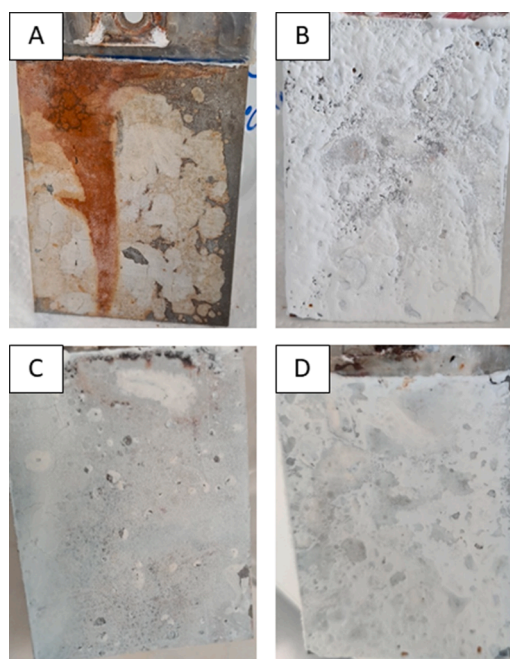
Fig. 5. A) Cathode after 14 days at 55 μA/cm^2, 7 °C, B) cathode after 14 days at 310 μA/cm^2, 22 °C, C) cathode after 14 days at 4 °C, 150 μA/cm^2, D) cathode after 14 days at 25 °C, 150 μA/cm^2.

Furthermore, the results of the adhesive test showed no correlation between the adhesive strength and composition of the deposited material for the tested samples. It indicates that the change in temperature and current do not influence the material's adhesive strength. Additionally, it was not possible to conduct the adhesive test on some samples containing a low amount of deposit produced at a low current density of 55 μA/cm^2.

3.1. Results from SEM and EDX analysis

SEM micrographs and corresponding overlaid EDX were used for identifying the crystal morphologies and elemental composition of the deposit materials subjected to changes in temperature and current densities.

The SEM and EDX analysis showed that the formation of brucite at a current density of 150 μA/cm^2 (cf. Fig. 6) is denser and more compact than brucite produced at a current density of 265 μA/cm^2 (cf. Fig. 7). The higher current density led to a higher production of hydrogen gas thus resulting in a porous structure. It was also observed during the collection of the deposited material on the cathode surface that the material produced at a higher current density (265 μA/cm^2) was softer and less cohesive compared to a lower current density.

The SEM images of sample F4 (cf. Fig. 8) show that the aragonite crystals in the deposited layer are well defined, intact and compact. On the other hand, sample F3 mainly consisting of brucite has a more porous structure than F4.

Further, analysing the SEM images of sample O1, aragonite crystals can be observed growing on top of the brucite layer confirmed by EDX (cf. Fig. 6). Findings from XRD analysis showed that about one third of the deposited material in sample O3 consists of aragonite.

3.2. Response surface model for aragonite

The model for aragonite content in the deposit on the cathode with current and temperature as factors can be observed in Eq. (3), where J and T are current density and temperature, respectively.
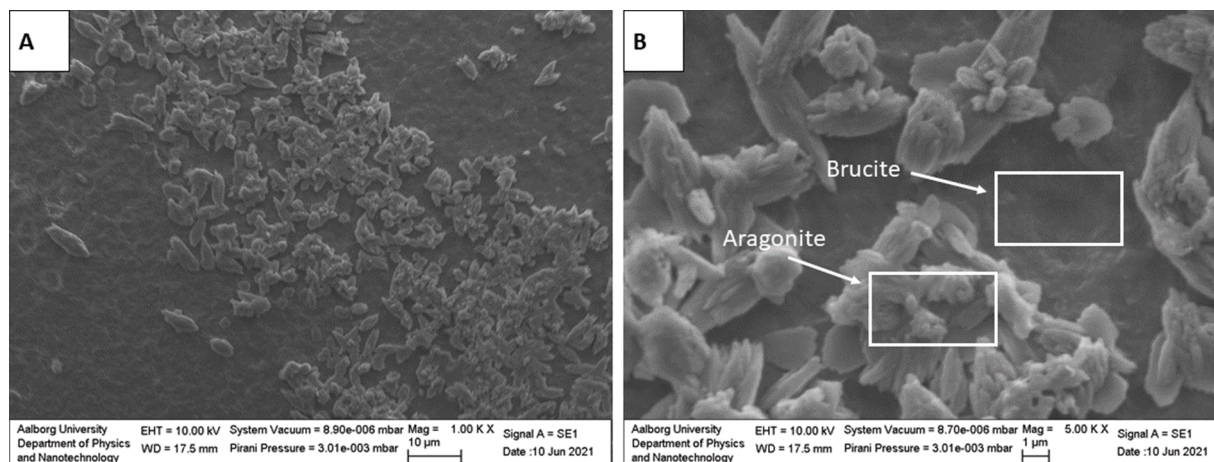
Fig. 6. SEM micrographs of sample O1 (4 °C, 150 µA/cm^2) A) magnification of 1000x B) magnification of 5000x. The needle like aragonite crystals is observed growing on top of the brucite layer supported by EDX.
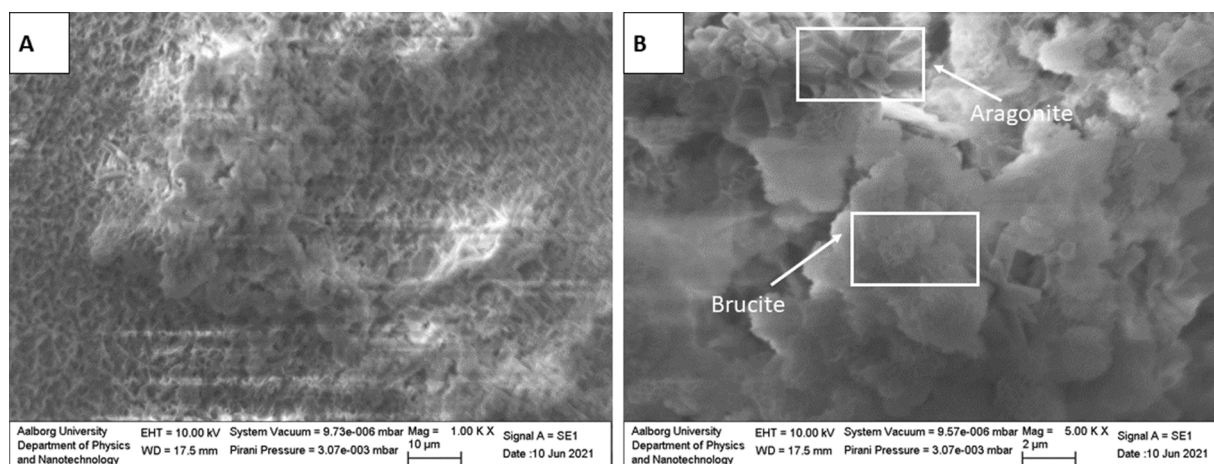

Fig. 7. SEM micrographs of sample F3 (7 °C, 265 µA/cm^2), A) magnification of 1000x B) magnification of 5000x. The hexagonal structures of aragonite crystals next to brucite were identified by EDX.
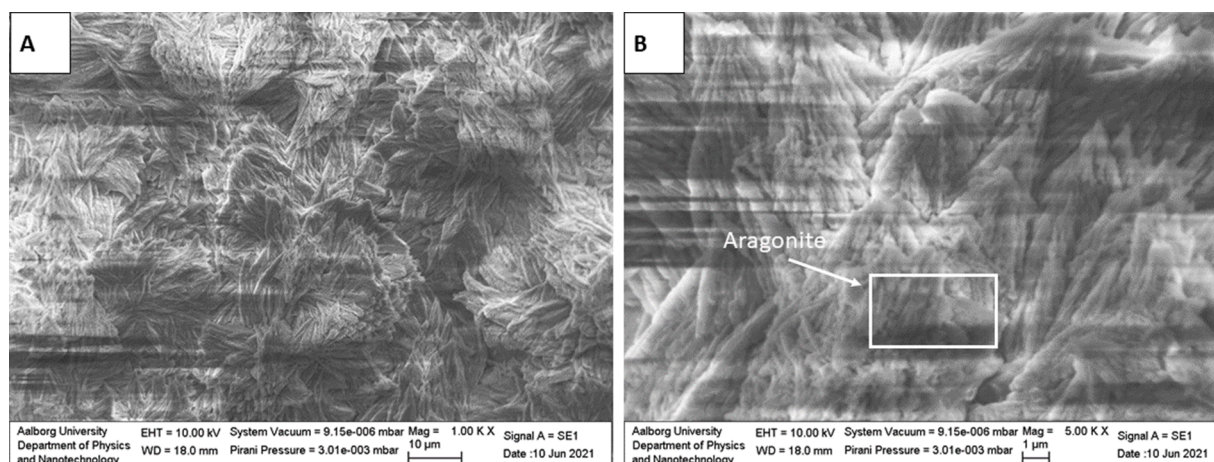

Fig. 8. SEM micrographs of sample F4 (7 °C, 55 µA/cm^2), A) magnification of 1000x, B) magnification of 5000x showing compact needle like aragonite crystals.

$$Aragonite[\%] = 156.647 - 1.058J - 3.499T + 0.005JT + 0.002J^2 + 0.065T^2$$

$$(3)$$

The model is based on the results from Table 3, containing twelve data points. The adjusted R^2 of the model is 0.968, where the quadratic term for current (J^2) and both independent variables (J and T) and the intercept are significant (p-value < 0.05). However, the quadratic term for temperature (T^2) and the interaction term JT resulted in p-values above the significance limit indicating a lack of statistical evidence for curvature effect from temperature on the percentage of aragonite in the

deposit.

Fig. 9 shows the mesh and contour plot for the aragonite percentage in the deposit. Observing the contour plot and the mesh plot for aragonite percentage, the highest amount is found at a low current density (55 μA/cm²) and lower temperature. With an increase in current density a lower aragonite percentage would be obtained in the calcareous deposit. Increasing the current density from 55 μA/cm² at 4 °C to 150 μA/cm² decreases the percentage of aragonite in the deposit from ~93% to ~35%. Further investigating the mesh and contour plot the model predicts that the amount of aragonite is the lowest at 18.2 °C and 230 μA/cm² with an aragonite percentage of 3.22%.

The potential governs the type of reaction occurring near the cathode, where the current controls the reaction rate. The increased current would also lead to an increased potential, following Ohms law, thus altering the deposit from aragonite to brucite. As discussed earlier the lower potential favours the formation of aragonite, whereas a higher potential favours the formation of brucite. The produced model observed in Eq. (3) and Fig. 9, follows the theory, until ~200 μA/cm² where a decrease in aragonite content would be observed with increased current. However, increasing the current further would not increase the amount of aragonite in the calcareous deposit. Furthermore, as stated previously, no calcareous deposit is formed below 55 μA/cm² due to a low overpotential, which was unable to initiate the redox reaction.

The solubility constant of aragonite increases with temperature reduction, meaning that aragonite's solubility lessens. Additionally, at a lower temperature the formation of brucite is less favoured [4]. This correlation is also observed in the model where a higher amount of aragonite is found at a lower temperature compared to a higher temperature.

Overall, the model showed that current and temperature significantly influence the percentage of aragonite in the composite material. The model predicted that the current densities within the range of ~55–115 μA/cm² at a given temperature ranging from 4 to 25 °C would provide a composite material with an aragonite percentage above 30%, which can reach up to 93% at 55 μA/cm² and 4 °C.

3.3. Response surface model for weight

A second response surface model has been generated from the data in Table 3 for the weight of the deposit with varying temperature and current (cf. Eq. (4)). In Eq. (4), J and T are current density and temperature, respectively.

$$Weight\left[\frac{g}{cm^3}\right] = -0.032 + 4.214 \cdot 10^{-4}J - 0.003T + 5.974 \cdot 10^{-6}JT$$
$$- 6.282 \cdot 10^{-7}J^2 - 6.773 \cdot 10^{-5}T^2 \qquad (4)$$

The adjusted R^2 for the model is 0.91 where only the term for J is significant (p-value <0.05). An increase in current density increases the weight of the deposit. The contour and mesh plot in Fig. 10 for the model of weight shows that a higher amount of weight deposited on the cathode is obtained at a higher J and T.

Further investigating the model, it fits with the theoretical aspect, showing that a higher amount is deposited with increased temperature and current. The rise in temperature increases the number of reactions per unit of time. Additionally, the increased current increases the number of electrons available per unit of time for the electrochemical reactions, thus increasing the reaction rate even further. However, as mentioned previously decreasing the applied current below 55 μA/cm², no calcareous deposit on the cathode can be formed.

The two responses of the weight of the calcareous deposit and the percentage of aragonite oppose each other, meaning there is no best optimum for both responses, however the aragonite percentage is determining the quality of the material deposited on the cathode. As previously stated, a strong material can be produced under CP, however brucite is a softer material compared to aragonite. Therefore, a higher strength of the material will be obtained at a lower current compared to a higher current, however with the cost of the obtained mass.

Overall, the electrochemical deposition of calcareous material has a great potential at reducing the required protective current density, thus facilitating a low-cost CP design. A study by Yasunobu et al. [25] investigated the relationship between calcareous coating thickness and protective current density. The obtained result showed that the required protective current density was significantly reduced when electro-coating thickness exceeded 0.1 mm regardless of the coating composition. The protective current density decreased from 118.7 μA/cm² to 13.0 μA/cm² only by the initial formation of 0.153 mm thick calcareous deposit, about one ninth of the required current density.

In the current study, it was observed that at minimum required current density of 55 μA/cm² for initiating the electrochemical reactions resulted in a growth of calcareous material with a thickness ≥ 0.1 mm on the steel surface. Initially at such low current density the steel plate immersed in synthetic seawater started corroding, which eventually stopped after few hours of cathodic polarisation due to the formation of protective coating composed of calcareous minerals. It could be explained by the Ohm's law, where at a constant current, an increase in
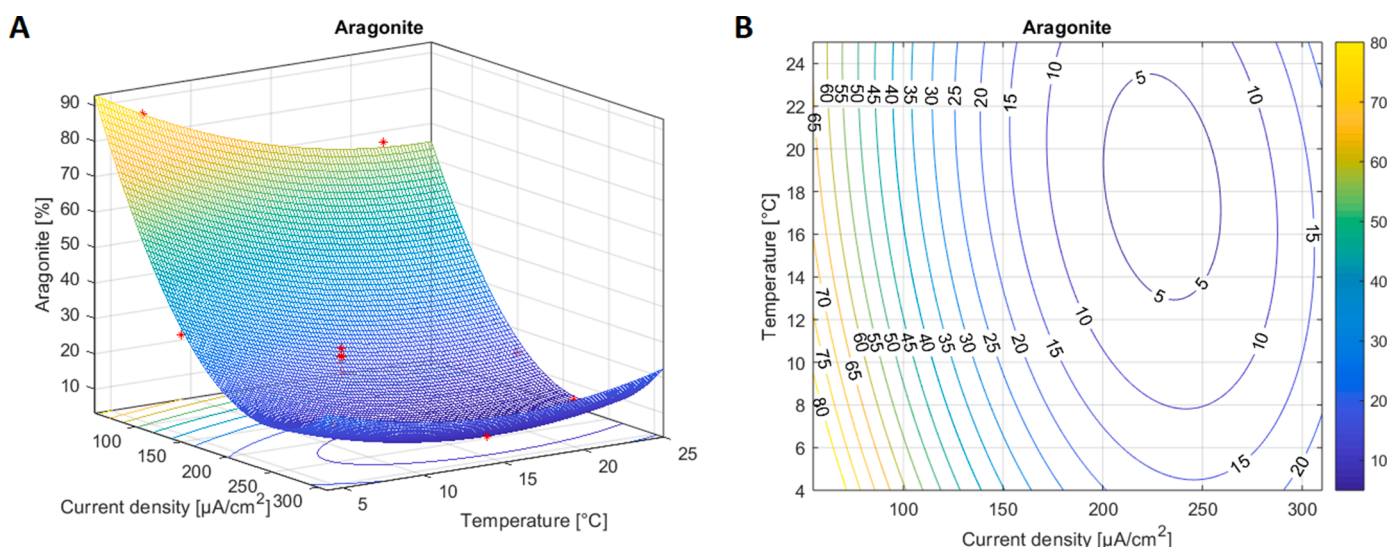

Fig. 9. A) mesh plot for aragonite percentage, plotted with the datapoints B) contour plot for aragonite percentage.
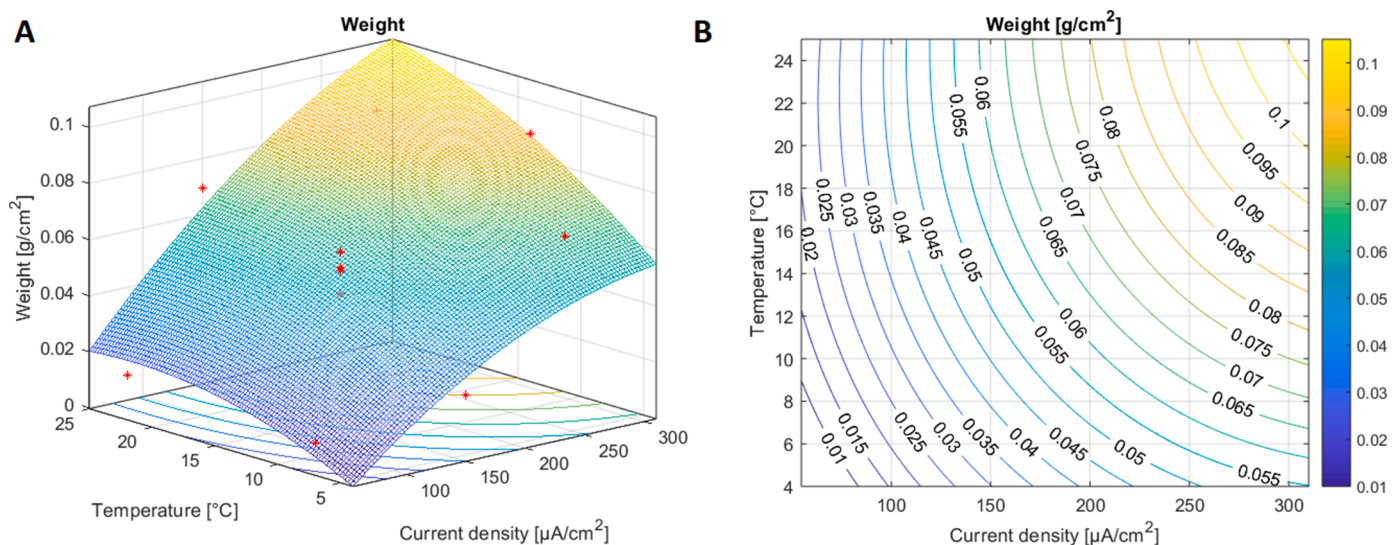
Fig. 10. A) Mesh plot for the weight of calcareous deposit, B) contour plot showing the weight of calcareous deposit on the cathode in g/cm^2.

the resistance due to the formation of iron oxides would increase the voltage exceeding the overpotential, thus initiating the redox reaction.

The models produced in this study can predict the composition and the amount of deposition per square centimetre within the range of 55 – 310 $\mu A/cm^2$ current density and 4 – 25 °C temperature. In addition, the water in the North Sea is typically within the temperature range of 3 – 19 °C, meaning that the model can be used to predict the amount of calcareous material deposited on offshore structures.

Formation of a thick, dense and compact calcareous coating can prevent the corrosion factors such as oxygen and seawater from diffusing towards the steel structure, thus significantly reducing the required proactive current density. The material itself is self-generating, if there is a loss of material due to erosion, the material can be regenerated without any human intervention. Furthermore, the models produced in this study can be implemented to predict the growth rate of initial layer of calcareous material with a certain ratio of $CaCO_3/Mg(OH)_2$ at a particular current density and temperature; thus, the protective current density can be regulated to a lower value. A very low protective current density may not be sufficient to provide cathodic protection to the offshore structures, however combining with an initial layer of calcareous material, the system can run more efficiently at a low protective current density.

4. Conclusion

Electrochemical deposition of calcareous material on carbon steel surface in artificial seawater was investigated by introducing response surface methodology into the experimental plan. The deposited material effectively inhibited the corrosion of a carbon steel plate at a low current density of 55 $\mu A/cm^2$. SEM-EDX and XRD analysis showed a higher percentage of aragonite deposited on the carbon steel cathode at a low current density (55 $\mu A/cm^2$) and low temperature (7 °C). In addition, SEM images showed that needle like aragonite crystals formed on top of the brucite layer.

The composition of the calcareous material had a significant influence on the morphology and porosity of the structure. Though the growth of calcareous material was faster at higher current density, excessive formation of H_2 gas resulted in a porous structure, which was observed through SEM. Higher current density also resulted in the formation of a higher percentage of brucite, which is comparatively a softer material than aragonite. On the other hand, the deposited material was very compact and dense at a lower current density due to the enhanced ratio of aragonite/brucite. A combined effect from CP and calcareous

deposit prevented the carbon steel plate from corroding, regardless of the composition of the deposited material.

In this paper, two response surface models has been developed, one for the weight of calcareous deposit and one for percentage of aragonite in the deposit with a coefficient of determination of ≥ 0.91. The applied current influences the weight of the calcareous material produced on the steel cathode. Additionally, the amount of aragonite in the calcareous product is mainly governed by the current, where a lower current favour the formation of aragonite. The models can predict the amount and composition of calcareous material forming on the carbon steel plate at 55 – 310 $\mu A/cm^2$ current density and 4 – 25 °C temperature.

CRediT authorship contribution statement

Tanzila Sharker: Investigation, Formal analysis, Methodology, Visualization, Writing – original draft. **Kenneth R. Simonsen:** Investigation, Formal analysis, Methodology, Visualization, Writing – original draft. **Lucia Margheritini:** Conceptualization, Writing – review & editing. **Sergey V. Kucheryavskiy:** Conceptualization, Writing – review & editing. **Morten E. Simonsen:** Conceptualization, Methodology, Supervision, Project administration, Funding acquisition, Writing – review & editing.

Declaration of Competing Interest

The authors declare that they have no known competing financial interests or personal relationships that could have appeared to influence the work reported in this paper.

Data availability

The raw/processed data required to reproduce these findings cannot be shared at this time as the data also forms part of an ongoing study.

Acknowledgements

Supplementary materials

Supplementary material associated with this article can be found, in the online version, at doi:10.1016/j.electacta.2023.141960.

References

[1] C.J. Li, M. Du, The growth mechanism of calcareous deposits under various hydrostatic pressures during the cathodic protection of carbon steel in seawater, RSC Adv. 7 (2017) 28819–28825, https://doi.org/10.1039/c7ra03709k.

[2] L. Margheritini, G. Colaleo, P. Contestabile, T.L. Bjørgård, M.E. Simonsen, C. Lanfredi, A. Dell'Anno, D. Vicinanza, Development of an eco-sustainable solution for the second life of decommissioned oil and gas platforms: the mineral accretion technology, Sustain (2020) 12, https://doi.org/10.3390/su12093742.

[3] Y. Yang, J.D. Scantlebury, E.V. Koroleva, A study of calcareous deposits on cathodically protected mild steel in artificial seawater, Metals (Basel) 5 (2015) 439–456, https://doi.org/10.3390/met5010439.

[4] C. Barchiche, C. Deslouis, O. Gil, P. Refait, B. Tribollet, Characterisation of calcareous deposits by electrochemical methods: role of sulphates, calcium concentration and temperature, Electrochim. Acta. 49 (2004) 2833–2839, https://doi.org/10.1016/j.electacta.2004.01.067.

[5] J.-F. Yan, R.E. White, R.B. Griffin, Parametric studies of the formation of calcareous deposits on cathodically protected steel in seawater, J. Electrochem. Soc. 140 (1993) 1275–1280, https://doi.org/10.1149/1.2220970.

[6] W.H. Hartt, C.H. Culberson, S.W. Smith, Calcareous deposits on metal surfaces in seawater - a critical review, Corrosion 40 (1984) 609–618, https://doi.org/10.5006/1.3581927.

[7] A. Neville, A.P. Morizot, Calcareous scales formed by cathodic protection - An assessment of characteristics and kinetics, J. Cryst. Growth. 243 (2002) 490–502, https://doi.org/10.1016/S0022-0248(02)01532-4.

[8] C. Li, M. Du, R. Gao, Influence of dissolved oxygen on the protectiveness and morphological characteristics of calcareous deposits with galvanostatic polarization, J. Ocean Univ. China. 16 (2017) 243–248, https://doi.org/10.1007/s11802-017-2933-4.

[9] VGB/BAW standard corrosion protection for offshore wind structures part 4: cathodic protection (CP), (2018). www.vgb.org (accessed August 4, 2021).

[10] C.-S. Lee, J. Kang, M.-H. Lee, Properties analysis of environment friendly calcareous deposit films electrodeposited at various temperature conditions in natural seawater, J. Korean Soc. Mar. Eng. 39 (2015) 779–785, https://doi.org/10.5916/jkosme.2015.39.7.779.

[11] A. Benedetti, L. Magagnin, F. Passaretti, E. Chelossi, M. Faimali, G. Montesperelli, Cathodic protection of carbon steel in natural seawater: effect of sunlight radiation,

Electrochim. Acta. 54 (2009) 6472–6478, https://doi.org/10.1016/j.electacta.2009.06.022.

[12] R.U. Lee, J.R. Ambrose, Influence of cathodic protection parameters on calcareous deposit formation, Corrosion 44 (1988) 887–891, https://doi.org/10.5006/1.3584961.

[13] C. Deslouis, D. Festy, O. Gil, G. Rius, S. Touzain, B. Tribollet, Characterization of calcareous deposits in artificial sea water by impedance techniques - I. Deposit of CaCO3 without Mg(OH)2, Electrochim. Acta. 43 (1998) 1891–1901, https://doi.org/10.1016/S0013-4686(97)00303-4.

[14] T.J.F. Goreau, P. Prong, Biorock electric reefs grow back severely eroded beaches in months, J. Mar. Sci. Eng. 5 (2017) 7–9, https://doi.org/10.3390/jmse5040048.

[15] T.J. Goreau, W.H. Sun, Marine ecosystem restoration: cost and benefits for coral reefs, World Resour. Rev. 17 (3) (2005) 375–409.

[16] H. Johra, L. Margheritini, Y. I.Antonov, K.M. Frandsen, M.E. Simonsen, P. Møldrup, R.L. Jensen, Thermal, moisture and mechanical properties of Seacrete: a sustainable sea-grown building material, Constr. Build. Mater. 266 (2021), 121025, https://doi.org/10.1016/j.conbuildmat.2020.121025.

[17] W. Mao, W.H. Hartt, B. Raton, Growth Rate of Calcareous Deposits Upon Cathodically Polarized Steel in Seawater, Sheraton Hotel, Boston Massachussetts, 1985. Paper number 317, Corrosion 85.

[18] C. Carré, A. Zanibellato, M. Jeannin, R. Sabot, P. Gunkel-Grillon, A. Serres, Electrochemical calcareous deposition in seawater. A review, Environ. Chem. Lett. 18 (2020) 1193–1208, https://doi.org/10.1007/s10311-020-01002-z.

[19] R.C. Cooke, P.E. Kepkay, The solubility of aragonite in seawater - I. Effect of pH and water chemistry at one atmosphere, Geochim. Cosmochim. Acta. 44 (1980) 1071–1075, https://doi.org/10.1016/0016-7037(80)90060-5.

[20] Standard ASTM D1141; American Society For Testing and Materials: Philadelphia, PA, USA, 1999.

[21] A.Y. Aydar, Utilization of Response Surface Methodology in Optimization of Extraction of Plant Materials, in: Statistical Approaches With Emphasis on Design of Experiments Applied to Chemical Processes, InTech, 2018, https://doi.org/10.5772/intechopen.73690.

[22] C.M. Todaro, H.C. Vogel, Fermentation and Biochemical Engineering Handbook, Elsevier Science & Technology Books, 2014, 3 ed. https://ebookcentral.proquest.com/lib/aalborguniv-ebooks/detail.action?docID=1663369.

[23] N. Aslan, Application of response surface methodology and central composite rotatable design for modeling and optimization of a multi-gravity separator for chromite concentration, Powder Technol. 185 (2008) 80–86, https://doi.org/10.1016/j.powtec.2007.10.002.

[24] C. Deslouis, D. Festy, O. Gil, V. Maillot, S. Touzain, B. Tribollet, Characterization of calcareous deposits in artificial sea water by impedances techniques: 2-deposit of Mg(OH)2 without CaCO3, Electrochim. Acta. 45 (2000) 1837–1845, https://doi.org/10.1016/S0013-4686(99)00403-X.

[25] S. Yasunobu, A. Kenichi, K. Kaoru, I. Masanori, Development of new anti-corrosion method (IECOS) for marine steel structures, IHI Eng. Rev. 41 (2008) 58–67.